MÆDICA - a Journal of Clinical Medicine

ORIGINAL PAPER

MAEDICA – a Journal of Clinical Medicine
2024; 19(3): 526-535
https://doi.org/10.26574/maedica.2024.19.3.526

Considerations on Image Preprocessing Techniques Required by Deep Learning Models. The Case of the Knee MRIs

A. BOTNARI[a], M. KADAR[b], J. M. PATRASCU[a]

[a]"Victor Babes" University of Medicine and Pharmacy, Timisoara, Romania

[b]"1 Decembrie 1918" University of Alba Iulia, Alba Iulia, Romania

ABSTRACT

Objectives: *This study aims to demonstrate the preprocessing steps for knee MRI images to detect meniscal lesions using deep learning models and highlight their practical implications in diagnosing knee conditions, especially meniscal injuries, often caused by degeneration or trauma. Magnetic resonance imaging (MRI) is key in this field, especially when combined with ligament evaluations, and our research underscores the relevance and applicability of these techniques in real-world scenarios. Importantly, our findings suggest a promising future for the diagnosis of knee conditions.*

Materials and methods: *We initially worked with DICOM-format images, the standard for medical imaging, utilizing the Python packages PyDicom and SimpleITK for preprocessing. We also addressed the NIfTI format commonly used in research. Our preprocessing methods, designed with efficiency in mind, encompassed modality-specific adjustments, orientation, spatial resampling, intensity normalization, standardization and conversion to algorithm input format. These steps ensure efficient data handling, accelerate training speeds, and reassure the audience about the effectiveness of our research.*

Results: *Our study processed PD-sagittal images from 188 patients to create a test set for training a deep learning segmentation model. We successfully completed all preprocessing steps, including accessing DICOM header information using hexadecimal encoded identifiers and utilizing SimpleITK for efficient handling of both 2D and 3D DICOM data. Resampling was performed for all 188 sets. Additionally, manual segmentation was conducted on 188 MRI scans, focusing on regions of interest (ROIs), such as normal tissue and meniscus tears in both the medial and lateral menisci. This involved contrast adjustment and precise hand-tracing of the structures within the ROIs, demonstrating the effectiveness and potential of our research in diagnosing knee conditions, and offering hope for the future of knee MRI diagnosis.*

Conclusions: *Our study introduces innovative preprocessing methods that have the potential to advance the field. By enhancing researchers' understanding of the importance of preprocessing steps, we anticipate that our techniques will streamline the preparation of standardized formats for deep learning model training and significantly benefit radiologists and orthopedic surgeons. These techniques could reduce time and effort in tasks like meniscal tear segmentation or localization, inspiring hope for more efficient and effective achievements in the field.*

Keywords: meniscus tear, deep learning model, MRI, preprocessing.

Address for correspondence:
alexei.botnari@umft.ro (A.B.) and mkadar@uab.ro (M.K.)

Article received on the 28th of June 2024 and accepted for publication on the 30th of August 2024

INTRODUCTION

Since its integration into clinical practice in the 1980s, magnetic resonance imaging (MRI) has emerged as the preferred imaging modality for diagnosing meniscal pathology, boasting detection rates of accuracy, sensitivity and specificity ranging from 85–95% (1, 2). Not limited to identification, the role of MRI has expanded to encompass crucial aspects such as determining the type, location and extent of meniscal tears. These detailed imaging findings provided by MRI significantly impact surgical approaches and guide patient management. In cases without prior surgery, a meniscal tear diagnosis on MRI relies on distinct indicators like increased intrasubstance signal breaching the articular surface or alterations in meniscal shape or size (3, 4). Menisci are crescent-shaped fibrocartilaginous structures that act as shock absorbers and stabilize the knee joint. When injured, they can cause pain, swelling and limited mobility. Detecting these injuries promptly is essential for effective treatment planning and preventing further damage (5).

Musculoskeletal imaging often involves assessing knee pathology, with a significant focus on meniscal lesions, whether degenerative or traumatic (6). Magnetic resonance imaging is the preferred modality for evaluating meniscal issues, especially in conjunction with ligament injuries (7). The standard MRI examination involves acquiring two-dimensional thin slices in axial, sagittal and coronal planes. Proton density (PD) and intermediate-weighted images with fat signal suppression offer optimal detection of meniscal lesions, including tears, displaced fragments and associated signs of migration (8, 9).

Radiology images, acquired differently from natural pictures, exhibit distinctive features depending on the modality (*e.g.*, computed tomography or MRI) and technical parameters used (10). Digital imaging and communications in medicine (DICOM) format, a standard in clinical medicine, contains metadata alongside pixel data, encompassing image acquisition details, scanner information and patient identification. Radiologists typically import this information into the picture archiving and communication system (PACS) for clinical assessment, often adjusting using third-party software (11).

Advancements in knowledge regarding meniscal pathology, MRI appearances and the application of artificial intelligence (AI) in medical imaging have become prominent. Artificial intelligence (AI), particularly deep learning, has shown the potential to enhance diagnostic accuracy and treatment (12, 13). Its utilization in MRI primarily focuses on segmentation and classification, with recent expansions into various measurement techniques, such as MR fingerprinting, denoising, super-resolution and image synthesis (14).

Digitized pathology images present challenges due to the abundance and variability caused by tissue preparation and digitization. Preprocessing steps focus on data reduction; variations may arise even in a single center's lab over time. To address this, preprocessing and complex modeling are employed to create a reliable diagnostic tool, considering potential image modifications as part of the preprocessing steps before training a DL model (15, 16).

This study aims to demonstrate the procedural steps involved in preprocessing knee MRI images using a deep learning model to segment, classify, or detect meniscal lesions. ❑

MATERIAL AND METHODS

This section illustrates the procedures for preprocessing images to achieve the ultimate format suitable for segmentation and training a deep learning model.

Patients' MRI acquisition

A standardized dataset was required to train a deep learning model for segmenting and detecting meniscus lesions. Following approval from the Ethical Council of the hospital, knee MRI scans were obtained from the PACS system at the County Emergency Hospital of Alba Iulia, Romania. The retrospective collection spanned from 2016 to 2019, comprising 224 scans in 2016, 151 in 2017, 151 in 2018 and 124 in 2019, totaling 650 knee MRI scans. Each knee MRI scan was accompanied by a radiology report containing descriptions and diagnoses.

All knee MRI examinations were conducted utilizing a Siemens Magneton Essenza with a magnetic field strength of 1.5 T. The protocol for knee MRI acquisition underwent annual modifications, remaining consistent in 2018 and 2019

(Table 1). At this stage, the data exhibited heterogeneity, requiring preprocessing.

MRI analysis

AB evaluated both the result report and images from each MRI scan (Figure 1). Demographic data (Table 2) were extracted and recorded in an Excel spreadsheet following the MRI analysis.

After assessing each MRI, we classified the scans into five categories: ACL, ACL + meniscus, meniscus, arthritis and normal (Figure 2). Initially, each MRI scan was evaluated by an experienced musculoskeletal radiologist who provided a detailed medical report. However, during the categorization of the MRI scans, evaluations were conducted by a different musculoskeletal radiologist and an experienced orthopedic sports surgeon. The study did not include MRIs that revealed other abnormalities, such as bone tumors or cysts. We used the included scans to train the deep learning model and standardize image formats. We utilized proton density turbo spin echo (TSE) fat saturation sagittal images to focus on the meniscus. The imaging parameters were as follows: repetition time 2800 ms, echo time 26 ms, section thickness 3 mm, fat saturation set to 1.5 and matrix size of 256 pixels × 256 pixels (180 mm × 180 mm).

The annotations, which included patients' name, age and personal information, underwent anonymization.

The initial images were in DICOM format, which stands for Digital Imaging and Communications in Medicine (DICOM). This is the most used data format for medical images. To preprocess such files, we used the Python packages

Year	2016	2017	2018	2019
Knee MRI protocols	PD TSE FS SAG T1 SE SAG PD TSE FS COR T1 TIRM TRA T2 WE TRA T2TSE SAG T2 TSE OBLI ACL	T1 SE SAG PD TSE FS SAG PD TSE FS COR PD TSE FS TRA T2 ME3D WE COR PD TSE DIXON SAG PD TSE DIXON SAG	PD TSE FS SAG T1 SE SAG PD TSE FS COR PD TSE FS TRA T2 DE3D WE SAG T2 ME2D SAG T2 TSE OBL COR ACL T2 TSE OBL SAG ACL	PD TSE FS SAG T1 SE SAG PD TSE FS COR PD TSE FS TRA T2 DE3D WE SAG T2 ME2D SAG T2 TSE OBL COR ACL T2 TSE OBL SAG ACl

MRI=magnetic resonance imaging; SAG=sagittal; COR=coronal; TRA=transversal; IW=intermediate weighted; PD=proton density; TSE=turbo spin-echo; TIRM=turbo inversion recovery magnitude; WE=water excitation; OBLI=oblique; ACL=anterior cruciate ligament; SE=spin echo; FS=fat-suppressed; ME=multiple echo; DE3D WE=double echo steady state

TABLE 1. Protocol of knee MRI acquisition *per* year

	2016	2017	2018	2019
Gender-male (%)	127 (56%)	78 (51.6%)	74 (49.0%)	60 (49.5%)
Age (mean/SD)	45.09 (16.69)	42.51 (14.95)	43.97 (16.33)	45.79 (14.36)
Laterality-right (%)	113 (50%)	74 (49.0%)	77 (50.9%)	61 (49.1%)
Total	224	151	151	124

SD=standard deviation

TABLE 2. Demographic data

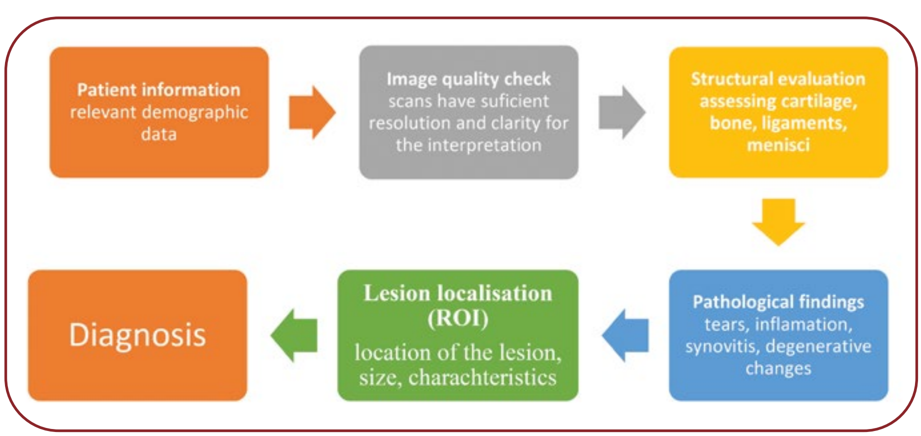

FIGURE 1. Workflow of the radiological assessment of knee MRIs

FIGURE 2. The sequence of processing knee MRI scans to reach a particular category image preprocessing

PyDicom and Simple ITK (17, 18). Another file format that is more used in research is NIfTI, which stands for Neuroimaging Informatics Technology Initiative (NIfTI) and has the advantage of being completely anonymous.

Preprocessing the datasets when applying deep learning is important to prepare for proper training and testing. Thus, we have applied various preprocessing techniques. These techniques are specific to modality, preprocess steps, normalization, standardization and homogenization of image resolution, size orientation and many more. Some deep learning methods may require specific input formats.

Finally, converting training data into more efficient data structures will increase the training speed due to decreased file access times.

The preprocessing steps include DICOM 1) modality-specific preprocessing; 2) orientation; 3) spatial resampling/resizing; 4) intensity normalization and standardization; and 5) conversion to algorithm input format.

Modality specific preprocessing

Modality-specific preprocessing deals with finding suitable processing techniques for all modalities. Even image reconstruction algorithms, which are supposed to convert the scanner's raw output into a form humans can understand, are part of those techniques. However, those algorithms are usually directly implemented in the scanner. Noise removal from the raw or the already reconstructed scanner outputs is another important task. There are some rare occasions when is necessary to apply denoising algorithms, but most of the time, the data we deal with is already denoised.

Complex artifacts might occur depending on the modality one works with. Motion is a much harder problem when working with CT or MRI data, but it is not that bad when the task of motion correction has its own research field, which is far too broad to be addressed within this paper. Sometimes, motion correction might already be implemented in the scanner.

The last point to mention is the importance of quantifying the outputs or, in other words, making sure that all outputs have the same unit. This technique is usually directly implemented in the scanner.

Orientation

Orientation-based preprocessing algorithms aim to achieve a standardized image orientation for the whole dataset. If one fails to handle this step, one might obtain a dataset in which the first axis sometimes moves from top to bottom and sometimes from left to right. Such a dataset will decrease your training performance and drastically worsen the results.

Resampling

When resampling, the goal is to get a standardized physical resolution and size. This means that all scans in the dataset have the same shape and all voxels in all scans have the same physical resolution. For example, each voxel might cover an area of one cross, one cross and one millimeter. If the single voxels already have the same physical resolution, this can be performed by resampling, padding, or cropping.

Normalization and standardization

The goal is to obtain standardized intensity values. By various methods such as modality-specific standardization to defined value intervals [(e.g. (-1,1)], normalization and standardization per subject (*e.g.*, MR) and standardization per dataset (e.g., knee MR).

For example, between -1 and 1 or zero and one, this procedure can simplify the learning process of the model. Depending on the task, it may increase the model's training, speed, performance, or even both. Different normalization or standardization techniques can usually be used. For example, when dealing with MRI data, one normalizes and standardizes per subject.

Table 3 provides an overview of the most common preprocessing techniques. When working with X-ray images, it is necessary to standardize the data by scaling those images with a constant of one divided by 255. After that, the mean and standard deviation of the whole dataset must be computed to perform set normalization. One typically does not need to perform normalization when dealing with CT images. However, scaling the data with a constant division of 3071 might increase performance. Additionally, depending on the task, one can use windowing or cropping.

Windowing is simply another word for contrast, enhancement, or contrast changes.

Conversion between input formats

After applying all necessary preprocessing steps, data might need to be converted to more convenient formats. When working on raw Dicom files, one should consider converting them to Nifti or another data format that can handle multidimensional data. Then, one might consider efficient data storage for deep learning pipelines. For example, one can convert data into numpy files or use efficient memory containers such as Hdf5 or SAR.

Annotation and labeling

The outcomes derived from manual segmentation are dependable when discerning structures for diagnosing knee disorders. ITK-SNAP 4.0.1 tool was employed for segmentation, representing an open-source application for manual and automated segmentation of various anatomical structures (19).

ITK-SNAP offers a platform for visualizing intricate 3D and four-dimensional (4D) imaging datasets and a toolkit for effectively and accurately labeling target structures (20). The visualization environment facilitates the simultaneous display of two-dimensional (2D) image cross-sections and 3D surface representations, enhancing spatial navigation in 3D images. This tool enabled us to work with multiple image datasets concurrently, even if they varied in resolution, orientation, or imaging modality. ❑

RESULTS

Manual classification

After evaluating each MRI scan, we classified each study into a distinct category. We selected only PD, T1 and T2 sequences for each category and organized them into separate folders. Initially, we had 650 MRI scans from data acquisition. Following the categorization, 610 MRI scans remained. Forty scans have been excluded due to containing other abnormalities, such as bone tumors or cysts. Table 4 summarizes the results after assessing each knee MRI scan.

Image preprocessing results

We have preprocessed the PD-sagittal images for 188 patients as a test set for the segmentation model training. The MRI scans for the test set were chosen from 2016 and 2017. Since we needed preprocessed images for a deep learning model to detect and segment the meniscus automatically, we specifically selected scans from the normal and meniscus subcategories. All preprocessing steps have been accomplished. We accessed the DICOM header information using the hexadecimal encoded identifiers at the start of each line. As an example, for the shape of the image, we used the following identifiers: (0028,

TABLE 3. Preprocessing techniques

	X-RAY images	(Body-) CT images	MRI images	PET images	Ultrasound
Normalization	Z-normalization (whole dataset)	-	Z-normalization (individual subject)	-	Z-normalization
Standardization	Scale with 1:255	Scale with 1:3071	Min-max scaling (individual subject)	Clip values at 20-40 scaling	Scale with 1:255
Task-specific-preprocessing		Windowing, cropping	Cropping	Log	

TABLE 4. The results of MRI scan categories

	NORMAL	MENISCUS	ARTHRITIS	ACL	ACL+MENISCUS	TOTAL
2016	22	82	61	14	22	201
2017	20	64	33	8	16	141
2018	23	63	34	11	12	143
2019	17	61	25	5	17	125
TOTAL	82	270	153	38	67	610

ACL=anterior cruciate ligament

0010) rows; (0028, 0011) columns; and (0018, 0015) body part examined.

The 0x before the identifier tells the Python interpreter to interpret this value as hexadecimal. The pixel array contains the actual image data, after accessing DICOM body information (the actual image) (Figures 3 and 4).

Then, a quick sanity check ensured that the image shape corresponded to the rows and columns as above-mentioned by us in the header information (256x256) (Figure 5).

Preprocessing 3D data

One hundred eighty eight patients have been processed with a 3D volume of 27 slices per patient. The 3D data has been stored as multiple 2D DICOM files. Typically, one file is for each slice. Thus, we must read all files and append the slices to a list.

It is possible that the DICOM files are not ordered according to their actual image position. In this case, it is necessary to inspect with SliceLocation attribute. It is crucial to order them, as otherwise, the complete scan would be shuffled and useless. The "SliceLocation" attribute is passed to the sorted function to identify the 2D slice position and thus order the slices (Figure 6).

We extracted the actual data (pixel arrays) from the DICOM files and stored them in a list. And now, we can look at some slices of the ordered 3D volume.

We handled 2D and 3D data stored in the DICOM format. However, manual file reading and ordering seemed tedious, so we used Simple ITK to handle all the images (18). SimpleITK provides functionality to automatically detect and read all DICOM files without managing the file reading or slice order. The overall routine is always identical by getting the series IDs of all files in the directory. This is important as multiple scans might be in the same directory, and we do not want to mix them.

ImageSeriesReader.GetGDCMSeriesIDs(path) handles this and returns all IDs it can find.

Then, we returned all file names in the directory with the desired ID.

ImageSeriesReader.GetGDCMSeriesFileNames (path, ID) provides this functionality.

We then defined the image reader called *ImageSeriesReader()* and fed it the file names using *SetFileNames(file_names)*.

Finally, we execute the reader to get our desired data by calling *Execute()* to get your full volumetric data. As one can see, the shape is (256, 256, 27), whereas above it is (27, 256, 256). This is just due to a different order of image dimensions.

```
(0028, 0010) Rows                                US: 256
(0028, 0011) Columns                             US: 256
(0018, 0015) Body Part Examined                  CS: 'KNEE'
```

FIGURE 3. Pixel array of image data

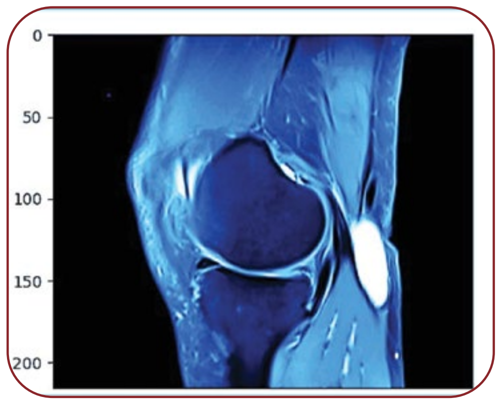

FIGURE 4. Accessing the pixel array of the DICOM file

```
print(ct.shape)
(256, 256)
```

FIGURE 5. Python sanity check

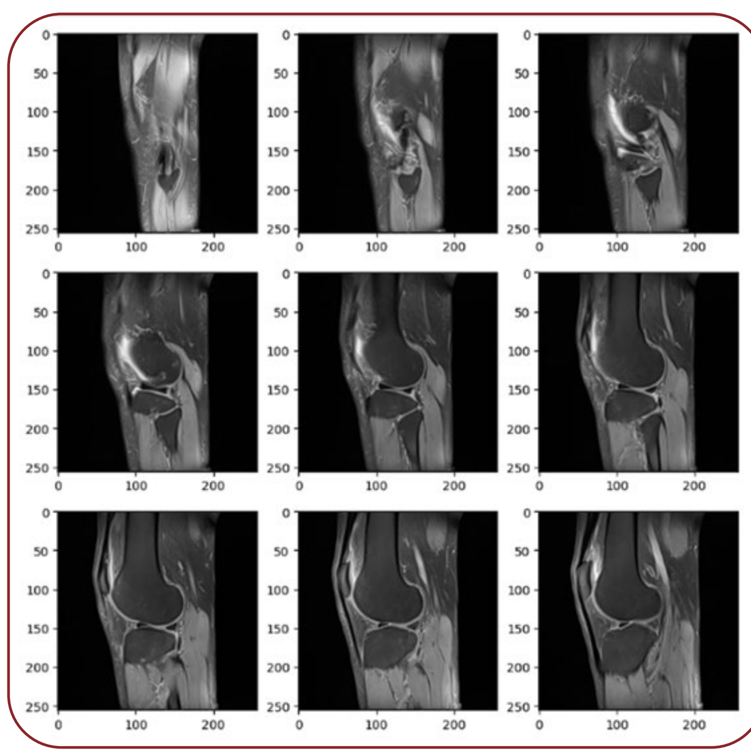

FIGURE 6. Example of the 3D volume of ordered slices

The final step is to convert the site image object to a NumPy array, which can be done by calling *GetArrayFromImage(image_data)*. It also directly moved the slice channel to the front. The result is shown in Figure 7.

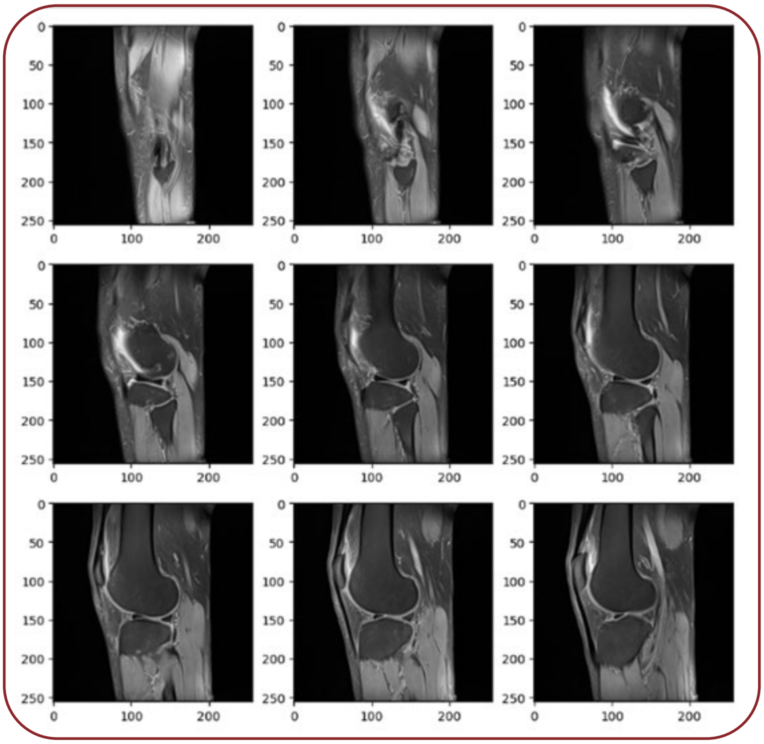

FIGURE 7. Example of ordered slices

```
import nibabel.processing

voxel_size = (2, 2, 2)
knee_mri_resized = nibabel.processing.conform(brain_mri, (128, 128, 100), voxel_size, orientation="PSR")
knee_mri_resized_data = brain_mri_resized.get_fdata()
```

```
print(knee_mri.shape)
print(knee_mri.header.get_zooms())

(25, 256, 256)
(3.5999997, 0.703125, 0.703125)
```

```
print(knee_mri.shape)
print(knee_mri_resized.shape)
print(knee_mri_resized.header.get_zooms())

(25, 256, 256)
(128, 128, 100)
(2.0, 2.0, 2.0)
```

FIGURE 8. Image resampling

Resampling

In some cases, it is required to change the size of the scan as it might be too large for the system. However, resizing a volume is not as easy as resizing an image because the voxel size needs to be changed. Resampling has been done for 188 sets with the code presented in Figure 8.

An example of a resampled image from 256 pixels to 128 pixels is shown in Figure 9.

Normalization

Images captured by MRI do not have an absolute, fixed scale and each patient varies. Thus, one can z-normalize the scans patient-wise. An example of z-normalization is given in Figure 10.

Annotation and labeling

After preprocessing the data, each proton density (PD) fast spin echo (FSE) with fat saturation (fs) MRI scan in NIFTI format was imported into ITK-SNAP. The sequence of images of each scan had a specific naming convention, such as P2016menisc1.nii.gz. Following segmentation, the corresponding segmented file was named P2016menisc1_seg.nii.gz. A total of 188 MRI scans were manually segmented by AB for each region of interest (ROI), encompassing normal or meniscus tears in the medial and lateral menisci. The initial step involved adjusting the contrast and manually segmenting each part of the medial and lateral menisci by zooming into the respective ROI. Manual segmentation was accomplished by hand-tracing the contour of the structure (Figure 11).

The 3D image offered high resolution in all spatial dimensions, while the 2D images exhibited excellent meniscus contrast across the three planes, as depicted in Figure 11a. Manual

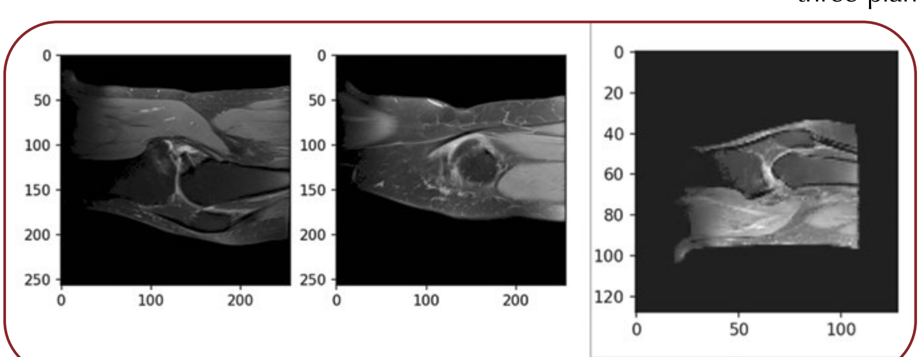

FIGURE 9. Resampling of images from 256 pixels to 128 pixels; knee MRI from (256, 256, 150) to (128, 128, 100)

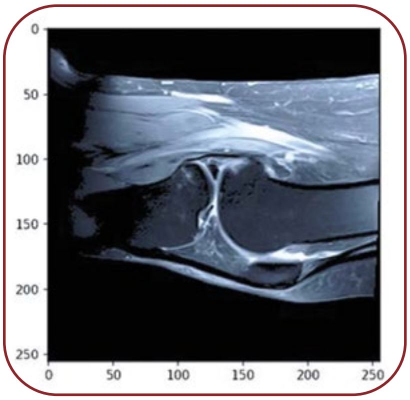

FIGURE 10. Z-normalization of the image

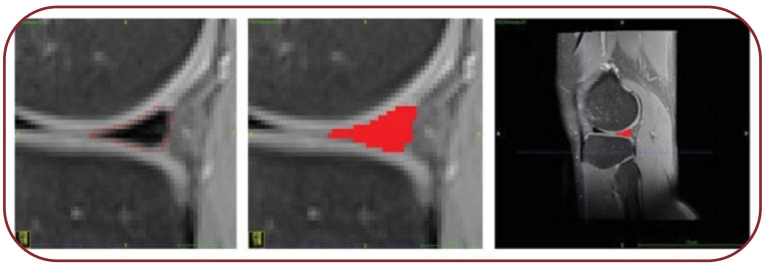

FIGURE 11. a) Image zooming in (annotation of posterior horn lateral meniscus); b) zooming in segmented posterior lateral meniscus; c) zooming out segmented posterior horn lateral meniscus

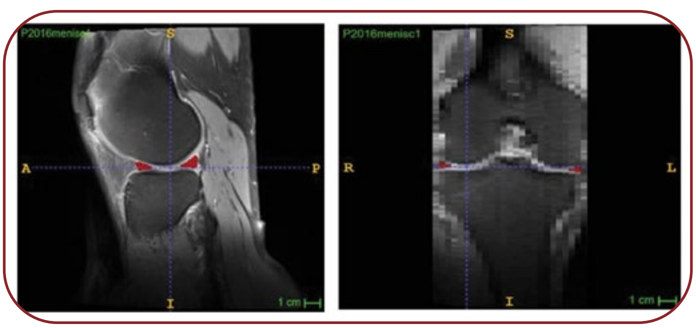

FIGURE 12. Manual segmentation of the menisci

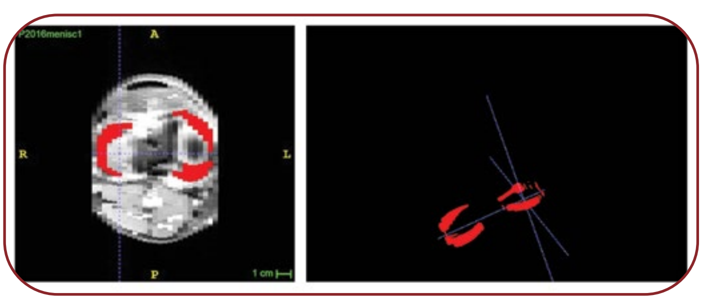

FIGURE 13. 3D reconstruction of the menisci

segmentation was executed on 2D proton density with fat saturation (PDFS) sequences in sagittal planes (Figure 12). A segmentation mask was generated for each sequence and a threshold value was set to encompass the menisci voxels. Background voxels were eliminated by cropping the segmentation mask to a box containing only the menisci. The segmentation mask underwent an opening morphological operation, followed by a region-growing operation, manual editing and further cropping. 3D meshes were computed from the masks in each sequence, resulting in low-resolution 3D representations of the menisci in all three planes. These three 3D representations were combined to form a unified model, smoothed to refine uneven surfaces. The solid 3D model was incorporated into the high-resolution 3D sequence and any necessary final manual editing was performed. ❑

DISCUSSIONS

Undoubtedly, radiology is a prominent domain witnessing the rise of artificial intelligence. Traditionally, radiologists and orthopedic surgeons have relied on their expertise and visual acuity to interpret medical images for diagnostic purposes. However, such tasks are labor-intensive and prone to significant errors. The existing limitations underscore the need for an alternative approach. The emergence of deep neural networks offers a promising avenue, allowing certain radiological tasks to be delegated to pre-trained machines (21). Nonetheless, the successful transition towards automation relies heavily on radiologists' comprehension of these algorithms. Deep neural networks are predominantly employed for various visual computation tasks in radiology, encompassing detection, classification and segmentation (22).

In due course, it becomes imperative for every orthopedic surgeon and radiologist to accurately define a problem in alignment with the capabilities of deep learning algorithms, procure and label relevant data that aligns with the algorithm's requirements to address the identified problem, execute essential preprocessing steps to refine the input data and select an appropriate algorithm.

Manual segmentation of the meniscus, ligaments, knee bones and cartilage often leads to intra-observer and inter-observer variations, posing challenges in clinical use and reproducibility (23). This tedious task necessitates developing a computer-aided diagnosis (CAD) system for automatically segmenting knee images, thereby reducing the burden on medical experts and minimizing variabilities. However, automating knee image segmentation is intricate due to varying intensity levels within tissue classes, small cartilage structures, image artifacts, low tissue contrast and shape irregularity (24).

In parallel, proton density (PD) imaging stands out for its remarkable contrast resolution, enabling precise differentiation of soft tissues like menisci, ligaments, and cartilage within the knee joint. Its sensitivity to water content further enhances diagnostic accuracy, particularly in detecting subtle meniscal abnormalities. PD imaging not only aids in accurate diagnosis but also guides timely interventions such as arthroscopic surgery or physical therapy, ultimately optimizing patient outcomes and healthcare delivery (25).

Concurrently, preprocessing techniques are vital in augmenting the reliability and efficacy of deep learning models applied to knee MRI images. These techniques encompass noise reduction, intensity normalization, image registration and spatial normalization, aiming to mitigate artifacts, enhance contrast and ensure consistency across datasets. Noise reduction techniques like Gaussian filtering and wavelet denoising enhance image clarity, facilitating accurate feature extraction crucial for identifying anatomical structures such as menisci and ligaments (26).

Furthermore, intensity normalization standardizes image intensities across diverse MRI scanners and protocols, reducing model bias and enhancing generalizability. For improved diagnostic accuracy, image registration and spatial normalization techniques align knee MRI images into a common coordinate space, facilitating direct comparison and fusion of multi-modal data.

Despite advancements, challenges persist, including parameter selection variability and the potential introduction of biases. Standardized preprocessing pipelines and exploration of advanced techniques such as generative adversarial networks are imperative for addressing these challenges and unlocking the full potential of deep learning in knee MRI analysis, thus revolutionizing patient care (27, 28). ❑

CONCLUSIONS

The literature lacks detailed descriptions of preprocessing techniques for image analysis using deep learning models. Our study aims to fill this gap by presenting novel preprocessing methods. We anticipate that our techniques will facilitate a deeper understanding of the criticality of preprocessing steps among researchers. Furthermore, we believe that adopting our methods will streamline the process for radiologists and orthopedic surgeons, reducing the time required to prepare standardized formats for training deep learning models in tasks such as meniscal tear segmentation or localization. ❑

Authors' contributions: A.B. and M.K. designed the study; A.B. collected the data; J.M.P. acted as a reviewer to resolve issues regarding knee MRI diagnosis for data synthesis; A.B. wrote the first draft and M.K. reviewed and updated the manuscript; M.K. provided input for the introduction, results, discussion and conclusions. All authors reviewed the manuscript, read it and agreed to its published version.

Acknowledgments: We acknowledge the Emergency County Hospital of Alba Iulia, Romania, for providing the knee MRI database from 2016 to 2019 following approval from the Ethical Board.

Conflicts of interest: none declared.

Financial support: none declared.

REFERENCES

1. **Nacey NC, Geeslin MG, Miller GW, Pierce JL.** Magnetic resonance imaging of the knee: An overview and update of conventional and state of the art imaging. *J Magn Reson Imaging* 2017;45:1257-1275. doi: 10.1002/jmri.25620.
2. **Stensby JD, Pringle LC, Crim J.** MRI of the Meniscus. *Clin Sports Med* 2021;40:641-655. doi: 10.1016/j.csm.2021.05.004.
3. **Gee SM, Posner M.** Meniscus Anatomy and Basic Science. *Sports Med Arthrosc Rev* 2021;29:e18-e23. doi: 10.1097/JSA.0000000000000327.
4. **Fox AJ, Wanivenhaus F, Burge AJ, et al.** The human meniscus: a review of anatomy, function, injury, and advances in treatment. *Clin Anat* 2015;28:269-287. doi: 10.1002/ca.22456.
5. **Renström P, Johnson RJ.** Anatomy and biomechanics of the menisci. *Clin Sports Med* 1990;9:523-538.
6. **Lecouvet F, Van Haver T, Acid S, et al.** Magnetic resonance imaging (MRI) of the knee: Identification of

difficult-to-diagnose meniscal lesions. *Diagn Interv Imaging* 2018;99:55-64. doi: 10.1016/j.diii.2017.12.005.

7. **Faruch-Bilfeld M, Lapegue F, Chiavassa H, Sans N.** Imaging of meniscus and ligament injuries of the knee. *Diagn Interv Imaging* 2016;97:749-765.
8. **Schaefer FK, Kurz B, Schaefer PJ, et al.** Accuracy and precision in the detection of articular cartilage lesions using magnetic resonance imaging at 1.5 Tesla in an in vitro study with orthopedic and histopathologic correlation. *Acta Radiol* 2007;48:1131-1137.
9. **Vande Berg BC, Lecouvet FE, Maldague B, Malghem J.** MR appearance of cartilage defects of the knee: preliminary results of a spiral CT arthrography-guided analysis. *Eur Radiol* 2004;14:208-214.
10. **Larobina M, Murino L.** Medical image file formats. *J Digital Imaging* 2014;7:200-206.
11. **McNitt-Gray MF, Pietka E, Huang HK.** Image preprocessing for a picture archiving and communication system. *Investig Radiol* 1992;27:529-535.
12. **Fayad LM, Parekh VS, de Castro Luna R, et al.** A deep learning system for synthetic knee magnetic resonance imaging: is artificial intelligence-based fat-suppressed imaging feasible? *Invest Radiol* 2021;56:357-368.
13. **Chaudhari AS, Grissom MJ, Fang Z, et al.** Diagnostic accuracy of quantitative multicontrast 5-minute knee MRI using prospective artificial intelligence image quality enhancement. *AJR Am J Roentgenol* 2021;216:1614-1625.
14. **Lundervold AS, Lundervold A.** An overview of deep learning in medical imaging focusing on MRI. *Z Med Phys* 2019;29:102-127.
15. **Smith B, Hermsen M, Lesser E, et al.** Developing image analysis pipelines of whole-slide images: Pre- and post-processing. *J Clin Transl Sci* 2020;5:e38. doi: 10.1017/cts.2020.531.
16. **Masoudi S, Harmon SA, Mehralivand S, et al.** Quick guide on radiology image preprocessing for deep learning applications in prostate cancer research. *J Med Imaging* (Bellingham) 2021;8:010901. doi: 10.1117/1.JMI.8.1.010901.
17. https://pydicom.github.io/pydicom/1.1/getting_started.html
18. https://simpleitk.org/SimpleITK-Notebooks/01_Image_Basics.html
19. **Virzì A, Muller CO, Marret J-B, et al.** Comprehensive Review of 3D Segmentation Software Tools for MRI Usable for Pelvic Surgery Planning. *J Digit Imaging* 2020;33:99-110.
20. http://www.itksnap.org/pmwiki/pmwiki.php?n=Downloads.SNAP4
21. **Bien N, Rajpurkar P, Ball RL, et al.** Deep learning-assisted diagnosis for knee magnetic resonance imaging: development and retrospective validation of MRNet. *PLoS Med* 2018;15:e1002699.
22. **Pedoia V, Norman B, Mehany SN, et al.** 3D convolutional neural networks for detection and severity staging of meniscus and PFJ cartilage morphological degenerative changes in osteoarthritis and anterior cruciate ligament subjects. *J Magn Reson Imaging* 2019;49:400-410.
23. **Starmans M, Zhou SK, Rueckert D, Fichtinger G.** Radiomics: Data mining using quantitative medical image features. Handbook of Medical Image Computing and Computer Assisted Intervention. Academic Press, Cambridge. 2020, pp 429-456.
24. **Kumar D, et al.** Knee Articular Cartilage Segmentation from MR Images: A Review. *ACM Comput Surv* 2018;51:1-29.
25. **Jerban S, Chang EY, Du J.** Magnetic resonance imaging (MRI) studies of knee joint under mechanical loading: Review. *Magn Reson Imaging* 2020;65:27-36. doi: 10.1016/j.mri.2019.09.007.
26. **Muncy NM, Hedges-Muncy AM, Kirwan CB.** Discrete preprocessing step effects in registration-based pipelines, a preliminary volumetric study on T1-weighted images. *PLoS One* 2017;12:e0186071. doi: 10.1371/journal.pone.0186071.
27. **Ahn G, Choi BS, Ko S, et al.** High-resolution knee plain radiography image synthesis using style generative adversarial network adaptive discriminator augmentation. *J Orthop Res* 2023;41:84-93. doi: 10.1002/jor.25325.
28. **Lv J, Wang C, Yang G.** PIC-GAN: A Parallel Imaging Coupled Generative Adversarial Network for Accelerated Multi-Channel MRI Reconstruction. *Diagnostics* (Basel) 2021;11:61. doi: 10.3390/diagnostics11010061.